ISSN 1063-7761, Journal of Experimental and Theoretical Physics, 2015, Vol. 120, No. 6, pp. 1024–1033. © Pleiades Publishing, Inc., 2015.
Original Russian Text © A.E. Sheyerman, K.Y. Constantinian, G.A. Ovsyannikov, Yu.V. Kislinskii, A.V. Shadrin, A.V. Kalabukhov, Yu.N. Khaydukov, 2015, published in Zhurnal Eksperimental'noi i Teoreticheskoi Fiziki, 2015, Vol. 147, No. 6, pp. 1185–1195.

ORDER, DISORDER, AND PHASE TRANSITION IN CONDENSED SYSTEM

Spin-Triplet Electron Transport in Hybrid Superconductor Heterostructures with a Composite Ferromagnetic Interlayer

A. E. Sheyerman[a,b], K. Y. Constantinian[a], G. A. Ovsyannikov[a,c], Yu. V. Kislinskii[a], A. V. Shadrin[a,b], A. V. Kalabukhov[c], and Yu. N. Khaydukov[d]

[a] *Kotelnikov Institute of Radio Engineering and Electronics, Russian Academy of Sciences, Moscow, 125009 Russia*
[b] *Moscow Institute of Physics and Technology, Dolgoprudny, Moscow oblast, 141700 Russia*
[c] *Chalmers University of Technology, Gothenburg, SE-41296 Sweden*
[d] *Max-Planck Institute for Solid State Research, Stuttgart, D-70569 Germany*
e-mail: karen@hitech.cplire.ru

Received October 29, 2014

Abstract—Hybrid $YBa_2Cu_3O_{7-x}/SrRuO_3/La_{0.7}Sr_{0.3}MnO_3/Au–Nb$ superconductor mesastructures with a composite manganite–ruthenate ferromagnetic interlayer are studied using electrophysical, magnetic, and microwave methods. The supercurrent in the mesastructure is observed when the interlayer thickness is much larger than the coherence length of ferromagnetic materials. The peak on the dependence of the critical current density on the interlayer material thickness corresponds to the coherence length, which is in qualitative agreement with theoretical predictions for a system with spit-triplet superconducting correlations. The magnetic-field dependence of the critical current is determined by penetration of magnetic flux quanta and by the magnetic domain structure, as well as by the field dependence of disorientation of the magnetization vectors of the layers in the composite magnetic interlayer. It is found that the supercurrent exists in magnetic fields two orders of magnitude stronger than the field corresponding to entry of a magnetic flux quantum into the mesastructure. The current–phase relation (CPR) of the supercurrent of mesastructures is investigated upon a change in the magnetic field from zero to 30 Oe; the ratio of the second CPR harmonic to the first, determined from the dependence of the Shapiro steps on the microwave radiation amplitude, does not exceed 50%.

DOI: 10.1134/S1063776115050192

1. INTRODUCTION

In 2001, it was shown theoretically that near the interface between a ferromagnet and a superconductor, triplet superconducting correlations (TSCs) with a nonzero spin projection occur in the ferromagnet near its interface with the superconductor along with conventional (singlet) correlations when the magnetization of the ferromagnet is spatially nonuniform [1, 2]. A distinguishing feature of TSCs is their insensitivity to the exchange field and their penetration to the bulk of the ferromagnet to distances typical of the normal (nonmagnetic) metal (up to 100 nm). The occurring TSCs were detected experimentally from the presence of supercurrent in the structure formed by two superconductors with singlet superconductivity, which are connected by a ferromagnetic interlayer with helical magnetization [3], and by a ferromagnetic film or nanowire with nonuniform magnetization at the interfaces with the superconductor [4, 5]. Later, it was proved theoretically that TSCs occur in a composite ferromagnetic interlayer between two singlet superconductors consisting of three and more ferromagnetic layers in which the extreme layers contacting with a superconductor ensure the conversion of the singlet component of superconducting correlations to the triplet correlation and back [6, 7]. Experiments on superconducting niobium structures with a composite cobalt-containing interlayer confirmed the possibility of such a process, although the questions concerning the mixing of compositions of metal layers remain unanswered [8, 9]. The reciprocal effect of TSCs on superconductivity in a singlet superconductor was detected in [10, 11]. TSCs in superconductor structures with a ferromagnetic interlayer consisting of two ferromagnets ($S/F_L/F_R/S$) were predicted for ballistic transport without barriers in asymmetric heterostructures with strongly differing thicknesses or exchange fields F_L and F_R of ferromagnets [12], as well as in the case of diffuse scattering [13, 14]. It was shown theoretically that the dominant second harmonic in the current–phase relation (CPR) of supercurrent is a manifestation of the long-range proximity effect [13, 15, 16]. The largest share of the second harmonic was predicted in [13] for disorientation of magnetizations F_L/F_S with an angle close to 90° and a thickness of one of the ferromagnets on the order of the coherence length ξ_F. It was concluded in [17] from data on the magnetic field dependence of critical current I_c that the second CPR harmonic dominates in SFS systems

with a magnetically active barrier. However, exact estimates of the contribution of the second harmonic to the CPR have not been obtained. An anomalously high value of the critical current, which has been observed in recent experiments with $YBa_2Cu_3O_{7-x}/SrRuO_3/La_{0.7}Sr_{0.3}MnO_3/Au–Nb$ structures, was explained by excitation of the triplet component of the supercurrent in the ferromagnetic interlayer [18, 19]. In most computations and experiments, a high transparency of interfaces (which is observed in experiments at the interface between metallic superconductors and metallic ferromagnets) was presumed. For example, in cuprate superconductor–manganite ferromagnet oxide structures, the transparency of the interface is determined, in particular, by the work function [20] and can be relatively low, which limits the proximity effect. It is for this reason that reports on the excitation of triplet correlations at the interface between a cuprate superconductor and manganite ferromagnet are rather contradictory. On the one hand, the occurrence of the triplet component in a manganite ferromagnet was reported [21–24], while on the other hand, the existence of a barrier with a low transparency at the interface between a cuprate superconductor and a manganite ferromagnet, which strongly limits the excitation of TSCs in the manganite ferromagnet, was detected [25, 26]. It should be noted that $La_{0.7}Sr_{0.3}MnO_3$ (LSMO) and $La_{0.7}Ca_{0.3}MnO_3$ (LCMO) manganite ferromagnets used in experiments are ferromagnets with 100% magnetic polarization of carriers (magnetic half-metals) at low temperatures. Therefore, singlet excitations at the interface with the ferromagnet are suppressed, but this does not rule out the excitation of spin-triplet correlations.

In this study, we report on the results of experimental investigations of supercurrent and quasiparticle current in hybrid epitaxial micron-size superconducting mesastructures with an asymmetric composite ferromagnetic interlayer; the characteristic quantities (in particular, the coherence length in the ferromagnet and transparency of the cuprate superconductor–ferromagnet interfaces) are estimated, and the contribution of the second harmonic in the current–phase relation of supercurrent is determined experimentally.

2. EXPERIMENTAL SAMPLES AND MEASURING TECHNIQUE

We studied mesastructures consisting of two superconductors (a cuprate superconductor with a high superconducting transition temperature and metallic niobium) connected by a composite interlayer consisting of two ferromagnets. The lower superconductor electrode ($YBa_2Cu_3O_{7-x}$ (YBCO) cuprate) was sputtered by laser ablation using an excimer Kr laser with a wavelength of 248 nm on (110)$NdGaO_3$ (NGO) or (001) $LaAlO_3$ (LAO) substrates with a size of 5×5 mm and a thickness of 0.5 mm; then two layers of ferromagnet (strontium ruthenate $SrRuO_3$ (SRO) and strontium-doped lanthanum manganite $La_{0.7}Sr_{0.3}MnO_3$ (LSMO)) were deposited in situ. The YBCO layer with a thickness of 80–190 nm was sputtered at a substrate temperature of 790°C and an oxygen pressure of 0.6 mbar; the SRO and LSMO layers were sputtered at a substrate temperature of 760°C and an oxygen pressure of 0.3 mbar. Then the mesastructure was cooled in an oxygen atmosphere to 100°C with a cooling rate of 5–10°C/min, after which the Au layer with a thickness of 20 nm was sputtered at a temperature of 100°C and a pressure of 10^{-5} mbar to prevent degradation of the surface prior to Nb sputtering ex situ during preparation of the mesastructure. A Nb layer with a thickness of 100 nm was deposited by magnetron sputtering [18]. The measuring circuit and the cross section of the mesastructure with a composite interlayer are shown in Fig. 1a. For comparison, structures with interlayers consisting of a single ferromagnet were prepared (Fig. 1b).

Depending on the sputtering conditions, the superconducting transition temperature for YBCO was 80–88 K for a transition width of 2 K. The upper superconducting electrode was an Au–Nb bilayer. The superconducting transition temperature of the bilayer was in the interval 8.3–8.7 K for a transition width of 0.2 K. Five mesastructures with linear sizes of $L = 10$, 20, 30, 40, and 50 μm on the plane were prepared on the substrate (henceforth referred to as a chip) using photolithography, ion-beam etching, and lift-off photolithography. The SiO_2 film of thickness 40 nm was used for insulating the contact at the end faces of the mesastructure. The properties of the surfaces were monitored for satellite films using an atomic force microscope, while sharp interfaces between SRO/LSMO layers were observed in the transmission electron microscope (Fig. 1c).

The use of the epitaxial film of the YBCO cuprate superconductor as the lower electrode was necessitated by the fact that this could ensure the epitaxial growth of the oxide interlayer, for which two ferromagnetic materials were used: LSMO with a coercive force of 20–30 mT and an exchange energy of 2.3 meV [27] and SRO with a coercive force on the order of 1 T and an exchange energy of 13 meV [28]. The resistive characteristics of satellite films and the current–voltage ($I–V$) characteristics of the mesastructures were measured using the four-probe circuit (see Fig. 1a) in the temperature range $4.2\ \text{K} < T < 300\ \text{K}$ in magnetic fields H up to 2 kOe under the action of microwave monochromatic radiation at frequencies $f_e = 1–3$ GHz and 36–45 GHz. Radiation with a frequency of 1–3 GHz was fed by a coaxial cable through blocking capacitors, while radiation of millimeter wavelengths was fed through a waveguide transmission line. To reduce the effect of external electric fields, measurements were taken in a screened box using a signal filtration system.

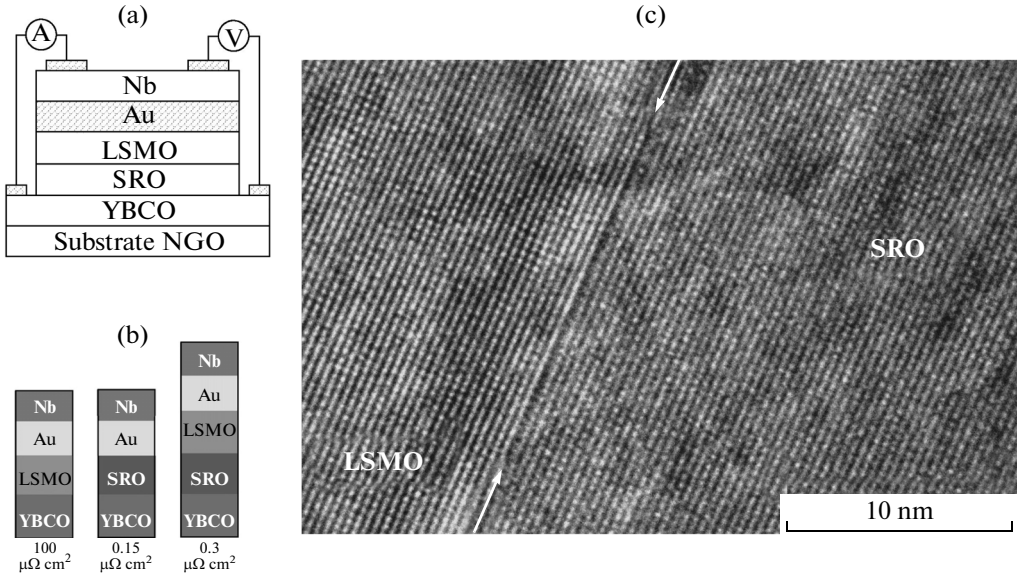

Fig. 1. (a) Cross section and circuit diagram for measuring electrophysical parameters of the mesastructure: A—source of current through the mesastructure; V—voltmeter. (b) Characteristic values of resistances R_NA for three types of mesastructure, averaged over five chips. (c) Image of the SRO/LSMO interface obtained by JEM-2100 transmission electron microscope with magnification 8×10^5; the position of the interface is marked by arrows.

3. EXPERIMENTAL RESULTS AND DISCUSSION

We tested more than 25 chips with a hybrid ferromagnetic interlayer with five mesastructures on each chip. The thicknesses of the SRO and LSMO films were varied in the limits of 4–23 and 2–28 nm, respectively. The topology of the chips remained unchanged; only the thicknesses of ferromagnetic interlayers were varied. The table contains the electrophysical parameters for several mesastructures that will be considered in greater detail below.

3.1. Electron Transport

The temperature dependences of resistance R of mesastructures (Fig. 2a) contain two segments with decreasing resistance, which correspond to transition of YBCO and Au–Nb films to the superconducting state. Above the superconducting transition temperature for YBCO (T_c^{YBCO}), the $R(T)$ dependence exhibits the metal-type linear behavior typical of the temperature dependence for the YBCO electrode (see Fig. 2b). At $T < T_c^{YBCO}$, the value of R sharply decreases (Fig. 2a) and no features typical of the temperature

Electrophysical parameters of mesastructures considered in this study

Mesastructure no.	d_{SRO}, nm	d_{LSMO}, nm	L, μm	R_NA, μΩ cm^2	j_c, A/cm^2	λ_J, μm
1	14	0	20	0.11	0	–
2	0	2	20	120	0	–
3	8.5	6	10	0.16	88	28
4	8.5	6	10	0.13	4.5	120
5	8.5	6	20	0.11	5.7	110
6	8.5	6	40	0.13	1.9	190
7	5.6	15	50	0.20	1.1	220
8	10	9	30	0.15	2.2	170
9	8.5	3	10	0.13	25	51

d_{SRO} and d_{LSMO} are the thicknesses of the SRO and LSMO films; L is the linear size of the mesastructure, j_c is the critical current density, R_NA is the characteristic resistance of the mesastructure, R_N is the normal resistance, and $A = L^2$ is the mesastructure area. Mesastructure nos. 4–6 are located on the same chip.

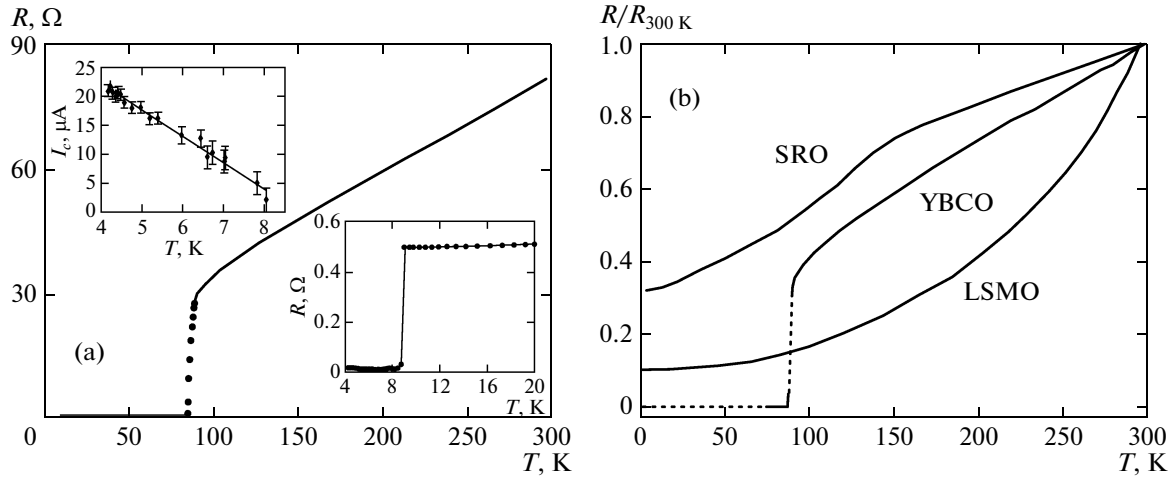

Fig. 2. (a) Temperature dependence of the resistance of mesastructure no. 8. The lower inset shows the magnified segment of the $R(T)$ curve at low temperatures; the upper inset shows the temperature dependence of the critical current. (b) Temperature dependences of normalized resistance of YBCO, SRO, and LMSO films with thicknesses of 100, 60, and 55 nm, respectively, sputtered directly on the (110) NGO substrate. The values of sheet resistances are 11, 27.5, and 87 Ω for YBCO, SRO, and LMSO films, respectively.

dependences of autonomous films (see Fig. 2b) constituting the mesastructures are observed in this temperature range. This is due to the fact that below the superconducting transition temperature of YBCO, the contribution of the LSMO and SRO films to the value of R_NA (area $A = L^2$) is substantially smaller than the contribution from the interfaces of the films in the mesastructure. Additional measurements show that the resistance of the Au–Nb bilayer film is also low [29]. As a result, the resistance of the mesastructure in the temperature range $T < T_c^{\mathrm{YBCO}}$ is the sum of the resistances of the YBCO/SRO, SRO/LSMO, and LSMO/Au interfaces between the materials:

$$R_{\mathrm{MS}} = R_{\mathrm{YBCO/SRO}} + R_{\mathrm{SRO/LSMO}} + R_{\mathrm{LSMO/Au}}.$$

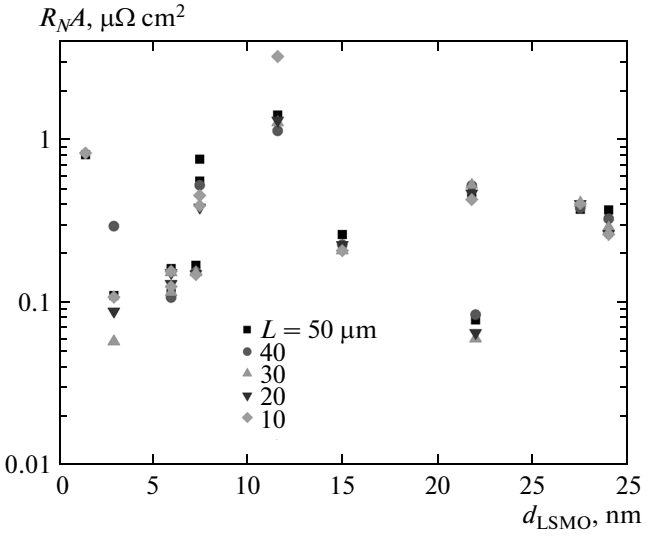

Fig. 3. Dependence of R_NA of the (110)NGO/YBCO/SRO/Au/Nb mesastructure on the thickness of the LSMO interlayer for various values of size L of the mesastructure.

Figure 3 shows the values of characteristic resistance R_NA of the YBCO/SRO/LSMO/Au–Nb mesastructures, measured for current $I > I_c$ of the mesastructure as a function of the LSMO interlayer thickness. It can be seen that the value of R_NA noticeably changes from chip to chip. The resistances of the mesastructures on the same chip (i.e., having the same thickness of the interlayer) differ much less strongly. It will be shown below that this is due to the decisive effect of the LSMO/Au interface, which was subjected to ion cleaning by ex situ sputtering of Nb, on the value of R_NA.

To compare the resistive characteristics of the interfaces in a mesastructure and to find which contribution from which interface determines the resistance of the mesastructure with a composite interlayer, we additionally prepared structures with a single ferromagnetic interlayer (e.g., sample nos. 1 and 2 in the table). The results for characteristic resistances R_NA averaged over five chips for all structures are shown in Fig. 1b. The value of R_NA for structures with the SRO interlayer is almost three orders of magnitude smaller than for the structure with the LSMO interlayer. Assuming that the resistance of the LSMO/Au interface does not exceed 1 μΩ cm² [30], the high resistance of the YBCO/LSMO/Au mesastructure (100 μΩ cm²) (see Fig. 1b) can be explained by the high resistance of the YBSO/LSMO interface. Using the results from [30], we find that the resistance of the SRO/Au interface is about 0.05 μΩ cm², while the

resistance to the YBCO/SRO interface is 0.1 μΩ cm^2, which coincides with the data from [25].

Let us consider the contribution from the LSMO/Au interfaces, which cannot exceed 0.2 μΩ cm^2 taking into account our results for the YBCO/SRO interface, which is smaller than the value obtained in [30] (1 μΩ cm^2). Note that data on the resistance of the LSMO/Au interface were obtained in [25, 30] by depositing gold ex situ after cooling of the LSMO epitaxial film transported to another chamber. As a result, the resistances of the LSMO/Au interface obtained by the two methods differ significantly. Consequently, the main contributions to the resistance of the mesastructure with a composite interlayer in our case comes from the interfaces ($R_{\mathrm{YBCO/SRO}} \approx 0.1$ μΩ cm^2 and $R_{\mathrm{LSMO/Au}} \approx 0.2$ μΩ cm^2).

We believe that resistance $R_{\mathrm{SRO/LSMO}}$ of the interface does not make a substantial contribution to the resistance of the mesastructure. TEM measurements show that the SRO/LSMO interface in mesastructures is quite homogeneous and is clearly seen on the scale of Fig. 1c. More detailed analysis of the SRO/LSMO interface using TEM with correction of aberrations in SRO/LSMO heterostructures [31] revealed mixing of Mn and Ru atoms on the scale of an atomic cell (0.3 nm), as well as mixing of Sr and La atoms on the scale of two atomic cells. Electron energy loss spectroscopy (EELS) revealed that a nonuniform distribution of oxygen vacancies within 1–2 nm can be observed at the SRO/LSMO interface [31, 32]. The high quality of the SRO/LSMO interface allows us to disregard the contribution of resistance $R_{\mathrm{SRO/LSMO}}$ of the interface. Indeed, analysis of superlattices $(\mathrm{LSMO/SRO})_n$ of the films (n = 1, 12, 24) revealed that the contribution of the resistance of the LSMO/SRO interface is substantially smaller than the resistance of individual films [33]. Consequently, the value of R_NA of the mesastructure is mainly determined by the resistances $R_{\mathrm{LSMO/Au}}$ and $R_{\mathrm{YBCO/SRO}}$.

Using the values obtained for the characteristic resistance of interfaces, we can estimate the averaged (over the directions of quasiparticle momentum) transparency of the LSMO/Au interface using the formula

$$D = \frac{2\pi^2\hbar^3}{e^2p_F^2}\frac{1}{R_NA} = \frac{2\rho^{\mathrm{LSMO}}l^{\mathrm{LSMO}}}{3R_NA}, \qquad (1)$$

where p_F is the smallest value of the Fermi momentum from LSMO and Au for the following parameters: $\rho^{\mathrm{LSMO}}l^{\mathrm{LSMO}} \approx 2\times10^{-11}$ Ω cm^2 and $R_NA = 0.2$ μΩ cm^2. The transparency D of the interface is found to be quite low ($D \approx 10^{-3}$). The transparency of the YBCO/SRO interface obtained for a slightly different characteristic resistance R_NA = 0.1 μΩ cm^2 of the interface is approximately equal to 10^{-2} due to smaller values of $\rho^{\mathrm{LSMO}}l^{\mathrm{LSMO}}$. It should be noted that the estimate for the transparency of the interface was obtained using the free electron model disregarding the correlation effects in metal oxide films. Consequently, we have a structure of two superconductors connected by a composite interlayer of two ferromagnets separated by a transparent interface. The transparency at the interfaces between the superconductors and ferromagnets is $D = 10^{-3}$ to 10^{-2}.

3.2. Dependence of the Critical Current on the Interlayer Thickness

The critical current observed for most investigated mesastructures with the total thickness of the composite interlayer from 7 to 50 nm in the temperature range 4.2 K < T < $T_c^{\mathrm{Au-Nb}}$ exhibited a linear decrease upon heating (see inset to Fig. 2a). For comparison, there was no supercurrent in mesastructures with a single ferromagnetic interlayer (LSMO or SRO) with a thickness exceeding 5 nm, which is equal in order of magnitude to the coherence length ξ_F, which will be estimated later. For smaller thicknesses of the interlayer, the supercurrent in some samples was associated with the current through pinholes. The existence and the power decrease of the critical current for composite layer thicknesses exceeding 5 nm indicate the transport of spin-triplet superconducting correlations through the ferromagnetic interlayer [8, 19]. The spread in the values of the critical current for different chips and within a chip noticeably exceeded the spread in the values of R_NA; for this reason, Fig. 4 shows the distribution profiles of the critical current density j_c on plane d_{LSMO}, d_{SRO}, which were obtained by averaging over several samples with the same thickness. It can be seen that the critical current density has a peak for layer thicknesses $d_{\mathrm{LSMO}} \approx 6$ nm and $d_{\mathrm{SRO}} \approx 8$ nm. It should be noted that the critical current peak of TSCs in superconducting structures with a bilayer composite ferromagnetic interlayer is predicted for a thickness on the order of the coherence length [7, 13].

Let us estimate the coherence length in the films forming the interlayer. Since electron mean free path l in oxide materials (SRO and LSMO) is quite small [35, 36], we can assume that the electron transport is of the diffusion type. In addition, thin films typically exhibit diffuse scattering from the SRO/LSMO interface due to the difference in the Fermi velocities of the materials. In the case of diffusion, the coherence length in a normal (nonferromagnetic) material is $\xi_N = (\hbar D/T)^{1/2}$, while its value in a ferromagnetic material is $\xi_F = (\hbar D/E_{\mathrm{ex}})^{1/2}$, where $D = v_Fl/3$ is the diffusion coefficient and v_F is the Fermi velocity. We can estimate the mean free path using the semiempirical formula $l = l_{\mathrm{phonon}}(R_{300\,\mathrm{K}}/R_{4.2\,\mathrm{K}} - 1)$, where l_{phonon} is the phonon mean free path from the literature (0.4 nm for LSMO [35] and 1 nm for SRO [36]). The measured $R(T)$ dependences show that $R_{300\,\mathrm{K}}/R_{4.2\,\mathrm{K}} \approx 3$ for SRO films grown on the (110)NGO substrate and $R_{300\,\mathrm{K}}/R_{4.2\,\mathrm{K}} \approx 10$ for LSMO films grown in the

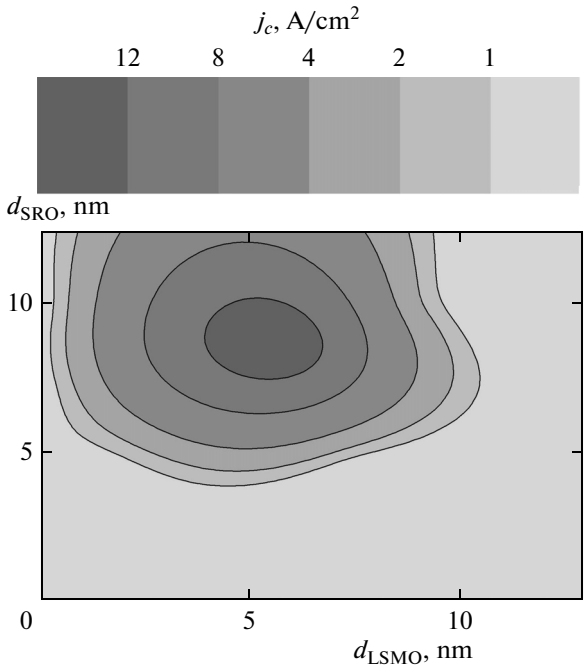

Fig. 4. Contours of the region of the critical current density distributions at $T = 4.2$ K on the plane of the thicknesses of the ferromagnetic layers of the interlayer. The boundaries are obtained from the values of j_c averaged over several mesastructures.

(110)NGO substrate (see Fig. 2b). This gives $\xi_F^{LSMO} \approx$ 8 nm and $\xi_F^{SRO} \approx 3$ nm, respectively. It can be seen from Fig. 4 that the peak of the critical current is observed for values of d_{LSMO} slightly smaller than our estimate of ξ_F^{LSMO}; conversely, the value of d_{SRO} for the SRO substrate is slightly larger than our estimates of coherence length ξ_F^{SRO}.

3.3. Magnetic-Field Dependences of the Critical Current

The magnetic-field dependences of the critical current of mesastructures (Fig. 5a) noticeably differed from the Fraunhofer dependence typical of Josephson junctions with a uniform distribution of the supercurrent. When the field direction changes (from an increase to a decrease and back), a hysteresis associated with the ferromagnetic origin of the interlayer materials is observed on a large scale of field variations. Moreover, the critical current is observed at much higher values of fields (up to 2 kOe in experiment; see inset to Fig. 5a). For example, for mesastructure no. 5 for $H = -1.3$ kOe, the critical current is $I_c = 16.5$ μA, which constitutes 94% of $I_c(H = 0)$ and 0.7 of the peak value at $H = -6.5$ Oe. It should be noted that the critical current in YBCO/Au/Nb mesastructures without a magnetic interlayer [29] and with an antiferromagnetic $Ca_{0.7}Sr_{0.3}CuO_2$ interlayer [37, 38] sharply decreased upon an increase in the magnetic field, while the critical current in a mesastructure with a ferromagnetic composite interlayer even increased in fields stronger than 1 kOe. Such an unusual behavior of the critical current with TSCs in structures with a metallic ferromagnetic interlayer was also noted in [9].

The magnetic-field dependence of the critical current is governed by several mechanisms: penetration of magnetic flux quanta (Josephson vortices) leading to the "Fraunhofer" dependence; the occurrence of the domain structure in the ferromagnetic interlayer; and rotation of the magnetization of the layers under the action of magnetic field. In the case of a Josephson junction with a uniform distribution of the supercurrent, the dependence of the critical current on the magnetic field parallel to the plane of the junction is described by the Fraunhofer dependence

$$I_c(H) = I_c(0)\left|\frac{\sin(\pi\Phi/\Phi_0)}{\pi\Phi/\Phi_0}\right|, \qquad (2)$$

where $\Phi_0 = 2.06783461 \times 10^{-7}$ G cm^2 is the magnetic flux quantum and $\Phi = \mu_0 H S_{eff}$ is the magnetic flux of the external field in the mesastructure [17, 39]. Zeros (minima) of the Fraunhofer dependence are observed for the external magnetic field flux through the cross section of the mesastructure, equal to magnetic flux quantum $\Phi \approx \Phi_0$. It should be noted that in the absence of TSC, the supercurrent must be considerably suppressed in a magnetic field in accordance with relation (2) for $\Phi \gg \Phi_0$, when several magnetic flux quanta penetrate the junction because the maxima on the Fraunhofer dependence decrease in proportion to $1/\Phi$.

Estimating the effective area $S_{eff} = Ld'$ of penetration of the magnetic field directed along the junction plane, we must take into account permeabilities of interlayers, $d' = \mu_1 d_{LSMO} + \mu_2 d_{SRO} + \lambda_{Nb} + \lambda_{YBCO}$, where $\lambda_{Nb} = 90$ nm and $\lambda_{YBCO} = 150$ nm, are the Londons magnetic field penetration depths for Nb and YBCO, respectively, and $\mu_{1,2}$ is the permeability. For Josephson junctions with a ferromagnetic interlayer, the effective thickness increases by a factor of $\mu = 1 + \chi$ [17, 40]. Substituting the values of $\mu_1 = 12$ and $\mu_2 = 3$ obtained from the magnetic-field dependences of the magnetic moment of the interlayer for thicknesses $d_{LMSO} = 6$ nm and $d_{SRO} = 8.5$ nm and $L = 10$ μm of mesastructure no. 4 (see Fig. 5a), we find that the minima of the critical current must be located at $\Delta H = 6$ Oe due to the penetration of Josephson vortices. This value differs insignificantly from spacing $\Delta H \approx 10$ Oe between the minima on the $I_c(H)$ curve shown in Fig. 5a. The difference can be due to the fact that to estimate χ, we used the results of measurements of magnetic moment $M(H)$, which were obtained for the magnetic field direction coinciding with the hard magnetization axis [19]. Fourier analysis of oscillatory dependences $I_c(H)$ recorded on the scale of fields up to

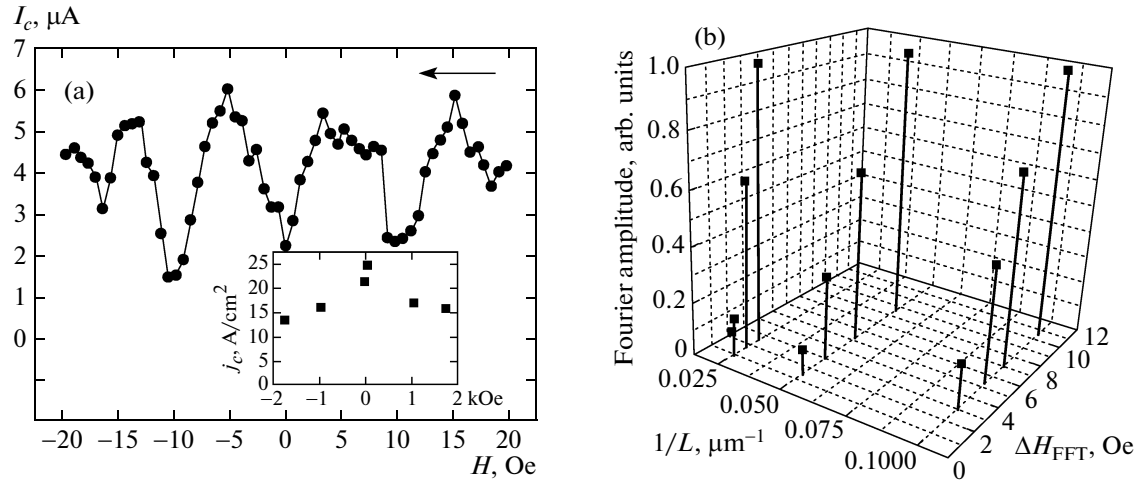

Fig. 5. (a) Magnetic-field dependence of the critical current in magnetic fields up to 20 Oe for mesastructure no. 4. The inset shows the dependence of the critical current peaks in a wide range of magnetic fields for mesastructure no. 9. (b) Periods ΔH_{FFT} and amplitudes of the Fourier components as functions of parameter $1/L$ for the magnetic-field dependences of the critical current for mesastructure nos. 4–6 located on the same chip.

±30 Oe for mesastructure nos. 4, 5, and 6 located on the same chip and having the same thickness d' shows the existence of three to five periods of the $I_c(H)$ dependence, which increase in proportion to L^{-1} (see Fig. 5b).

It is well known that the domain structure in the ferromagnetic interlayer can radically change the mechanism of electron transport [41–43]. In particular, domains can stimulate excitation of TSC in the ferromagnet in contact with a cuprate superconductor exhibiting d-wave symmetry of the superconducting order parameter [41]. Magnetic domains in the LSMO film in a magnetic field applied in the substrate plane have size $d_{\text{dom}} = 0.1$–0.3 μm, and the shape of domains strongly depends on the field strength in the film [44, 45]; the domains in the SRO film have the same size [46]. In weak magnetic fields (smaller than the LMSO saturation field approximately equal to 200 Oe), the domains of the LMSO film can produce the strongest effect, while in fields of 1000 Oe and higher, the domains in the SRO field play the major role. It should be noted that period d_{dom} of the domain structure is considerably smaller than the magnetic field penetration depths $\lambda_J = \Phi_0/(2\pi\mu_0 d' j_c)^{-1/2}$ in the Josephson junction, which are given in the table. According to estimates obtained in [43], magnetic flux distortions caused by domains are averaged over scale λ_J and are not manifested in the critical current for $d_{\text{dom}} \ll \lambda_J$. It cannot be ruled out, however, that domain-induced inhomogeneities in the magnetization of the LSMO film may lead to additional modulation of the $I_c(H)$ dependence. However, it can be seen from the data presented in Fig. 5b that the oscillations of $I_c(H)$ are not associated with the domain structure, because the effective area $S_{\text{eff}} = d_{\text{dom}} d'$ of magnetic field penetration in this case must correspond to substantially larger periods of oscillations of the critical current as a function of the magnetic field, than the value of ΔH_{FFT} in the figure. The existence of Fourier expansion components with fractional periods ΔH_{FFT} rather indicates the deviation of the CPR from the sinusoidal dependence [17] than the effect of the domain structure.

It is also important that the maximal values of the critical current are observed in nonzero magnetic fields (see Fig. 5a). In zero magnetic field, the coupling between the SRO and LSMO films is antiferromagnetic, as follows from the measurements of magnetization of YBCO/SRO/LSMO/Au samples on a SQUID magnetometer [19]. With increasing field, the angle between the directions of magnetization of the interlayer materials changes and the critical current increases [13]. In the LSMO saturation fields (200–300 Oe), the magnetization of LSMO is directed along the external magnetic field and does not change in strong magnetic fields. Consequently, the behavior of $I_c(H)$ in fields exceeding 1 kOe is determined by the magnetization of the SRO interlayer.

3.4. Microwave Dynamics of Mesastructures

Analysis of the high-frequency dynamics of the Shapiro steps occurring on the I–V curves under the action of microwave radiation indicates the lack of direct contacts (pinholes) between superconductors, because oscillations of Shapiro steps depending on the microwave power are observed and the amplitudes of these oscillations are conform with the model of a resistively shunted Josephson junction [29]. The absence of pinholes is ensured by high values of the interlayer thickness for which the roughness of the layers is much smaller than the thicknesses of the LSMO and SRO films.

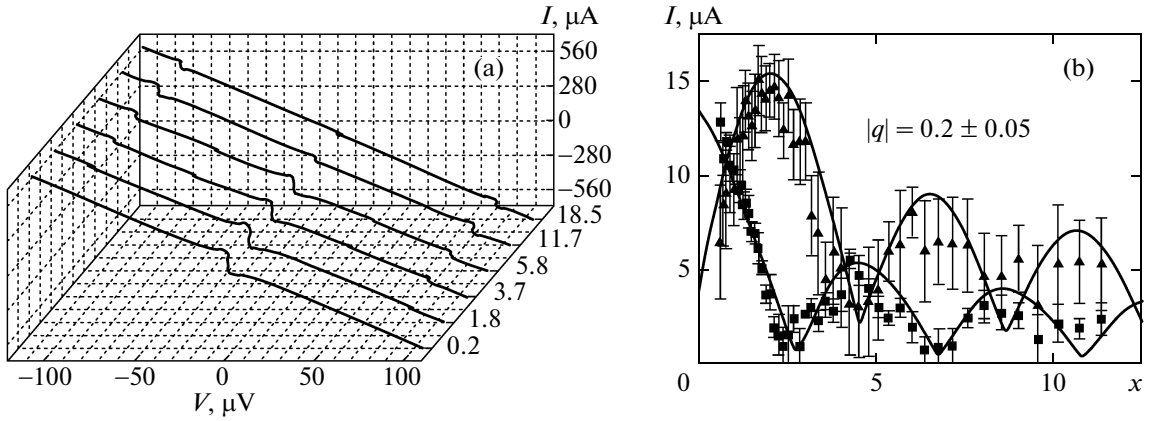

Fig. 6. (a) Family of I–V curves for mesastructure no. 3 under the action of electromagnetic radiation with a frequency of 41 GHz; $a = I_{RF}/I_c$. (b) Dependences of the critical current amplitudes (■) and the first Shapiro step (▲) of mesastructure no. 7 under the action of microwave radiation of frequency 3 GHz on $x = I_{RF}/I_c\omega$ at $T = 4.2$ K; $H = 133$ Oe.

A more accurate comparison of the experimental dependences of the Shapiro steps with those calculated using the modified resistive model [29] makes it possible to determine the CPR of mesastructures. The CPRs were measured in zero magnetic field as well as upon cooling of mesastructures in a constant magnetic field (100–200 Oe) parallel to the substrate plane. The family of I–V curves obtained under the action of microwave irradiation at a frequency of 41 GHz is shown in Fig. 6a. Since the normalized frequency f_e of microwave radiation was substantially higher than the characteristic frequency of the mesastructures ($f_e \gg f_c = (2e/h)I_cR_N$), the effect of capacitance of the mesastructures could be disregarded (McCumber parameter $\beta_c = (2\pi/\Phi_0)I_cR_N^2C \ll 1$). Under such conditions, the occurrence of a fractional Shapiro step on the I–V curve (which was determined by differentiating the I–C characteristics shown in Fig. 6a) unambiguously indicates that the CPR is not sinusoidal [29]. The ratio $q = I_{c2}/I_{c1}$ of the CPR second harmonic amplitude to the amplitude of the first harmonic was determined from numerical approximation of the dependences of the critical current amplitudes and Shapiro steps on the normalized microwave current (Fig. 6b). Due to the effect of the CPR second harmonic, the critical current and the first Shapiro step have nonzero local minima (see Fig. 6b). Since we assumed that $I_{c1} \approx I_c$ (which is the case for small $q < 1$), the values of q determined by this method are slightly underestimated. According to theoretical work [13], the second harmonic dominates in the CPR during the excitation of spin-triplet correlations in the asymmetric ferromagnetic interlayer, increasing with the angles of misorientation of magnetization of the layers in the interlayer and attaining its maximal value for angles close to $\pi/2$. According to the results of measurements on the SQUID magnetometer, antiferromagnetic ordering of the magnetizations of the LSMO and SRO layers is observed in the substrate plane. Consequently, in zero external field, the magnetizations of the ferromagnetic layers are antiparallel, and the critical current is minimal in accordance with the results obtained in [13]. This is indeed observed on the $I_c(H)$ dependence (see Fig. 5a). For the LSMO ferromagnet with uniaxial magnetic anisotropy, the angle between the direction of magnetization and the external magnetic field is determined by the magnetic field magnitude; in fields stronger than the saturation field (200–300 Oe), the magnetization of the LSMO layer is directed along the field. Consequently, an increase in the CPR second harmonic should be observed even in weak fields. However, we have not observed an increase in the fraction of the second harmonic in the microwave experiments on five mesastructures upon the application of a magnetic field of 20–50 Oe, and the maximal value was $q = 0.5$. The limitation imposed on the growth of the CPR second harmonic amplitude can be due to nonuniformity of the exchange field in the ferromagnetic layers, which is associated with the domain structure [42], as well as diffuse scattering and spin flip [14] because of the imperfection of the interfaces between the superconductors and ferromagnets in the mesastructure. It should be noted that the reason for the occurrence of the CPR second harmonic in a Josephson junction between the *s*-wave and *d*-wave superconductors can be due to the fact that the symmetry of the condensate wavefunction of YBCO in the *ab* plane is predominantly of the *d*-wave type [29]. However, in the *c* direction of YBCO, the critical current is determined by the *s*-wave component of the superconducting order parameter [29]. In our *c*-oriented mesastructures, the *s*-wave component of the YBCO is small, which is manifested in small values of critical frequency f_c as compared to that for structures without an interlayer [29]. It should be noted that in the *c* direction of superconducting contacts with the *d*-wave symmetry, which are connected by a ferromagnet

with a domain wall, exactly the *s*-wave TSC component appears [41]. However, the effect of the domain structure of ferromagnets on the ratio of the CPR harmonics of the Josephson current with TSCs in the $S/F_L/F_R/S$ junctions remains unclear.

4. CONCLUSIONS

It has been shown experimentally that the critical current of superconducting mesastructures with an LMSO/SRO asymmetric composite magnetic interlayer is a nonmonotonic function of thicknesses d_{LSMO} and d_{SRO} of the manganite and the ruthenate. The supercurrent is observed for the total interlayer thickness up to 50 nm (in particular, when $d_{LSMO} \gg \xi_F^{LSMO}$). The maximal critical current density is observed for interlayer thicknesses close to the coherence length. In spite of the low transparency of the interfaces between the superconductors and ferromagnets, the observed Josephson effect can be explained by the occurrence of TSCs. A complex magnetic-field dependence of the critical current of mesastructures is determined by several factors. For fields weaker than the saturation field for the LSMO film, Fourier analysis makes it possible to single out components corresponding to fractional values of the main period of $I_c(H)$ oscillations associated with deviation of the CPR from the sinusoidal dependence. This is confirmed by microwave measurements of the dependences of the Shapiro step heights on the radiation power; it was found that the value of the second harmonic may reach 50% of the first harmonic. Another factor determining the modulation of the magnetic-field dependence is the formation of domains; however, the mechanism of the influence of domains on the magnetic-field dependence of the critical current remains unclear so far.

ACKNOWLEDGMENTS

This study was supported financially by the Physics Division of the Russian Academy of Sciences, the President of the Russian Federation (grant no. NShf-4871.2014.2), Russian Foundation for Basic Research (project nos. 14-07-00285a and 14-07-93105), and the Vysby Program of the Swedish Institute.

The transmission electron microscope image was obtained using the equipment of the Center of Collective Usage "Nanotechnology" at the Moscow Institute of Physics and Technology.

The authors are grateful to I.V. Borisenko, D. Winkler, A.F. Volkov, V.V. Demidov, A.V. Zaitsev, L. Mustafa, and A.M. Petrzhik for their help in experiments and fruitful discussions.

REFERENCES

1. F. S. Bergeret, A. F. Volkov, and K. B. Efetov, Phys. Rev. Lett. **86**, 4096 (2001).
2. A. Kadigrobov, R. I. Shekhter, and M. Jonson, Europhys. Lett. **54**, 394 (2001).
3. J. W. A. Robinson, J. D. S. Witt, and M. G. Blamire, Science (Washington) **329**, 59 (2010).
4. M. S. Anwar, F. Czeschka, M. Hesselberth, M. Porcu, and J. Aarts, Phys. Rev. B: Condens. Matter **82**, 100501 (2010).
5. J. Wang, M. Singh, M. Tian, N. Kumar, B. Liu, C. Shi, J. K. Jain, N. Samarth, T. E. Mallouk, and M. H. W. Chan, Nat. Phys. **6**, 389 (2010).
6. M. Houzet and A. I. Buzdin, Phys. Rev. B: Condens. Matter **76**, 060504 (2007).
7. A. F. Volkov and K. B. Efetov, Phys. Rev. B: Condens. Matter **81**, 144522 (2010).
8. M. A. Khasawneh, T. S. Khaire, C. Klose, W. P. Pratt, Jr., and N. O. Birge, Supercond. Sci. Technol. **24**, 024005 (2011).
9. C. Klose, T. S. Khaire, Y. Wang, W. P. Pratt, Jr., N. O. Birge, B. J. McMorran, T. P. Ginley, J. A. Borchers, B. J. Kirby, B. B. Maranville, and J. Unguris, Phys. Rev. Lett. **108**, 127002 (2012).
10. P. V. Leksin, N. N. Garif'yanov, I. A. Garifullin, Ya. V. Fominov, J. Schumann, Y. Krupskaya, V. Kataev, O. G. Schmidt, and B. Büchner, Phys. Rev. Lett. **109**, 057005 (2012).
11. V. I. Zdravkov, J. Kehrle, G. Obermeier, D. Lenk, H.-A. Krug von Nidda, C. Müller, M. Yu. Kupriyanov, A. S. Sidorenko, S. Horn, R. Tidecks, and L. R. Tagirov, Phys. Rev. B: Condens. Matter **87**, 144507 (2013).
12. L. Trifunovic, Z. Popović, and Z. Radović, Phys. Rev. B: Condens. Matter **84**, 064511 (2011).
13. C. Richard, M. Houzet, and J. S. Meyer, Phys. Rev. Lett. **110**, 217004 (2013).
14. B. Sperstad, J. Linder, and A. Sudbo, Phys. Rev. B: Condens. Matter **78**, 104509 (2008).
15. L. Trifunovic, Phys. Rev. Lett. **107**, 047001 (2011).
16. M. Kneževi ć, L. Trifunovic, and Z. Radović, Phys. Rev. B: Condens. Matter **85**, 094517 (2012).
17. A. Pal, Z. H. Barber, J. W. A. Robinson, and M. G. Blamire, Nat. Commun. **5**, 3340 (2014).
18. G. A. Ovsyannikov, A. E. Sheierman, A. V. Shadrin, Yu. V. Kislinskii, K. Y. Constantinian, and A. Kalabukhov, JETP Lett. **97** (3), 145 (2013).
19. Yu. N. Khaydukov, G. A. Ovsyannikov, A. E. Sheyerman, K. Y. Constantinian, L. Mustafa, T. Keller, M. A. Uribe-Laverde, Yu. V. Kislinskii, A. V. Shadrin, A. Kalabukhov, B. Keimer, and D. Winkler, Phys. Rev. B: Condens. Matter **90**, 035130 (2014).
20. S. Yunoki, A. Moreo, E. Dagotto, S. Okamoto, and S. S. Kancharla, Phys. Rev. B: Condens. Matter **76**, 064532 (2007).
21. C. Visani, Z. Sefrioui, J. Tornos, C. Leon, J. Briatico, M. Bibes, A. Barthélémy, J. Santamaría, and J. E. Villegas, Nat. Phys. **8**, 539 (2012).
22. T. Hu, H. Xiao, C. Visani, Z. Sefrioui, J. Santamaria, and C. C. Almasan, Phys. Rev. B: Condens. Matter **80**, 060506R (2009).
23. Y. Kalcheim, T. Kirzhner, G. Koren, and O. Millo, Phys. Rev. B: Condens. Matter **83**, 064510 (2011).
24. T. Golod, A. Rydh, V. M. Krasnov, I. Marozau, M. A. Uribe-Laverde, D. K. Satapathy, Th. Wagner,

and C. Bernhard, Phys. Rev. B: Condens. Matter **87**, 134520 (2013).

25. M. van Zalk, A. Brinkman, J. Aarts, and H. Hilgenkamp, Phys. Rev. B: Condens. Matter **82**, 134513 (2010).
26. A. M. Petrzhik, G. A. Ovsyannikov, A. V. Shadrin, K. I. Konstantinyan, A. V. Zaitsev, V. V. Demidov, and Yu. V. Kislinskii, J. Exp. Theor. Phys. **112** (6), 1042 (2011).
27. B. F. Woodfield, M. L. Wilson, and J. M. Byers, Phys. Rev. Lett. **78**, 3201 (1997).
28. I. Asulin, O. Yuli, G. Koren, and O. Millo, Phys. Rev. B: Condens. Matter **79**, 174524 (2009).
29. P. Komissinskiy, G. A. Ovsyannikov, K. Y. Constantinian, Y. V. Kislinski, I. V. Borisenko, I. I. Soloviev, V. K. Kornev, E. Goldobin, and D. Winkler, Phys. Rev. B: Condens. Matter **78**, 024501 (2008).
30. L. Mieville, D. Worledge, T. H. Geballe, R. Contreras, and K. Char, Appl. Phys. Lett. **73**, 1736 (1998).
31. A. Y. Borisevich, A. R. Lupini, J. He, E. A. Eliseev, A. N. Morozovska, G. S. Svechnikov, P. Yu, Y.-H. Chu, R. Ramesh, S. T. Pantelides, S. V. Kalinin, and S. J. Pennycook, Phys. Rev. B: Condens. Matter **86**, 140102(R) (2012).
32. M. Ziese, I. Vrejoiu, E. Pippel, P. Esquinazi, D. Hesse, C. Etz, J. Henk, A. Ernst, I. V. Maznichenko, W. Hergert, and I. Mertig, Phys. Rev. Lett. **104**, 167203 (2010).
33. M. Ziese, F. Bern, A. Setzer, E. Pippel, D. H. Hesse, and I. Vrejoiu, Eur. Phys. J. B **86**, 42100 (2013).
34. F. V. Komissinskii, G. A. Ovsyannikov, and Z. G. Ivanov, Phys. Solid State **43** (5), 801 (2001).
35. J. L. Cohn, J. J. Neumeier, C. P. Popoviciu, K. J. McClellan, and Th. Leventouri, Phys. Rev. B: Condens. Matter **56**, R8495 (1997).
36. P. Kostic, Y. Okada, N. C. Collins, Z. Schlesinger, J. W. Reiner, L. Klein, A. Kapitulnik, T. H. Geballe, and M. R. Beasley, Phys. Rev. Lett. **81**, 2498 (1998).
37. Yu. V. Kislinskii, K. Y. Konstantinian, G. A. Ovsyannikov, F. V. Komissinsky, I. V. Borisenko, and A. V. Shadrin, J. Exp. Theor. Phys. **106** (4), 800 (2008).
38. V. V. Bol'ginov, V. S. Stolyarov, D. S. Sobanin, A. L. Karpovich, and V. V. Ryazanov, JETP Lett. **95** (7), 366 (2012).
39. A. Barone and G. Paterno, *Physics and Applications of the Josephson Effect* (Wiley, New York, 1982; Mir, Moscow, 1984).
40. G. Wild, C. Probst, A. Marx, and R. Gross, Eur. Phys. J. B **78**, 509 (2010).
41. A. F. Volkov and K. B. Efetov, Phys. Rev. Lett. **102**, 077002 (2009).
42. Ya. V. Fominov, A. F. Volkov, and K. B. Efetov, Phys. Rev. B: Condens. Matter **75**, 104509 (2007).
43. A. I. Buzdin, A. S. Mel'nikov, and N. G. Pugach, Phys. Rev. B: Condens. Matter **83**, 144515 (2011).
44. R. Desfeux, S. Bailleul, A. Da Costa, W. Prellier, and A. M. Haghiri-Gosnet, Appl. Phys. Lett. **78**, 3681 (2001).
45. J. Dho, Y. N. Kim, Y. S. Hwang, J. C. Kim, and N. H. Hur, Appl. Phys. Lett. **82**, 1434 (2003).
46. M. S. Anwar, F. Czeschka, M. Hesselberth, M. Porcu, and J. Aarts, Phys. Rev. B: Condens. Matter **82**, 100501 (2010).

Translated by N. Wadhwa